



OPEN

Large-range Control of the Microstructures and Properties of Three-dimensional Porous Graphene

SUBJECT AREAS:

MECHANICAL AND
STRUCTURAL PROPERTIES
AND DEVICESSTRUCTURE OF SOLIDS AND
LIQUIDS

GRAPHENE

STRUCTURAL PROPERTIES

Xiao Xie*, Yilong Zhou*, Hengchang Bi, Kuibo Yin, Shu Wan & Litao Sun

SEU-FEI Nano-Pico Center, Key Laboratory of MEMS of Ministry of Education, Southeast University, 210096 Nanjing, China.

Received
8 April 2013Accepted
13 June 2013Published
2 July 2013Correspondence and
requests for materials
should be addressed to
L.T.S. (slt@seu.edu.cn)* These authors
contributed equally to
this work.

Graphene-based three-dimensional porous macrostructures are believed of great importance in various applications, e.g. supercapacitors, photovoltaic cells, sensors and high-efficiency sorbents. However, to precisely control the microstructures and properties of this material to meet different application requirements in industrial practice remains challenging. We herein propose a facile and highly effective strategy for large-range tailoring the porous architecture and its properties by a modified freeze casting process. The pore sizes and wall thicknesses of the porous graphene can be gradually tuned by 80 times (from 10 to 800 μm) and 4000 times (from 20 nm to 80 μm), respectively. The property experiences the changing from hydrophilic to hydrophobic, with the Young's Modulus varying by 15 times. The fundamental principle of the porous microstructure evolution is discussed in detail. Our results demonstrate a very convenient and general protocol to finely tailor the structure and further benefit the various applications of porous graphene.

Graphene is a two-dimensional novel material with promising properties, such as excellent mechanical features, high conductivity and a large specific surface area^{1,2}. Three-dimensional, porous graphene-based macrostructures, i.e. porous graphene, may benefit from these properties to achieve outstanding performances and has received worldwide attention. There have been numerous reports every year showing remarkable features of porous graphene, such as low density ($\sim 180 \mu\text{g cm}^{-3}$)³, large specific surface area (up to 3100 $\text{m}^2 \text{g}^{-1}$)^{4,5}, and satisfactory electrical conductivity ($\sim 100 \text{ S m}^{-1}$)^{6,7}, etc. Consequently, graphene macrostructures have been extensively applied in various applications, such as electrodes⁸, energy storage units in supercapacitors⁹, bio- and gas sensors^{10,11}, etc. More attractively, porous graphene has been reported as efficient sorbent which removes oil and organic liquid pollution from water^{12,13}.

Depending on the need for an initial template (e.g., nickel foam), the fabrication of porous graphene can be divided into template-dependent and template-free protocols. The former strategy can generate porosity with extremely low densities and well-controlled porous structures^{3,9}, but it suffers from problems such as high cost, low yields and template residue after etching. Template-free strategy is much cheaper and more suitable for massive production^{12,13}. Freeze casting is a recently developed template-free strategy for graphene sponge fabrication. However, how to freely regulate the shape and microstructures in a large range remains unknown.

Freeze casting has been a novel approach for generating bulky, porous materials, such as ceramics^{14–17} and carbon nanotube¹⁸ structures. Much attention has been paid into the direct synthesis of porous materials based on the constant temperature of the cold source. It remains unknown how to precisely regulate the pore size and shape of the porous structures by this method. Moreover, little knowledge regarding the effects of freezing temperature on forming microporosity during the fabrication process has been acquired. Therefore, this study aims to improve freeze casting method for tailoring the structures of porous graphene materials and further explore the feasibility and mechanism of freeze-casting induced structure control during the fabrication of porous graphene.

In our previous work, graphene oxide (GO) as raw material was self-assembled into porous graphene through hydrothermal reduction and freeze casting. We demonstrated that water-resistant porous graphene, named as graphene sponge, can be used as effective absorbers for removing the organic solution of oil pollution¹³. In this report, we attempted to control the porous microstructures of graphene sponges by changing the parameters during freeze casting, especially the freezing temperature. Thus, the novel properties of graphene sponges, such as water absorption/resistance and mechanical features, could be obtained. The results of the present study show that, among the other parameters, the crystalline states of ice inside the sponges during freezing process plays the

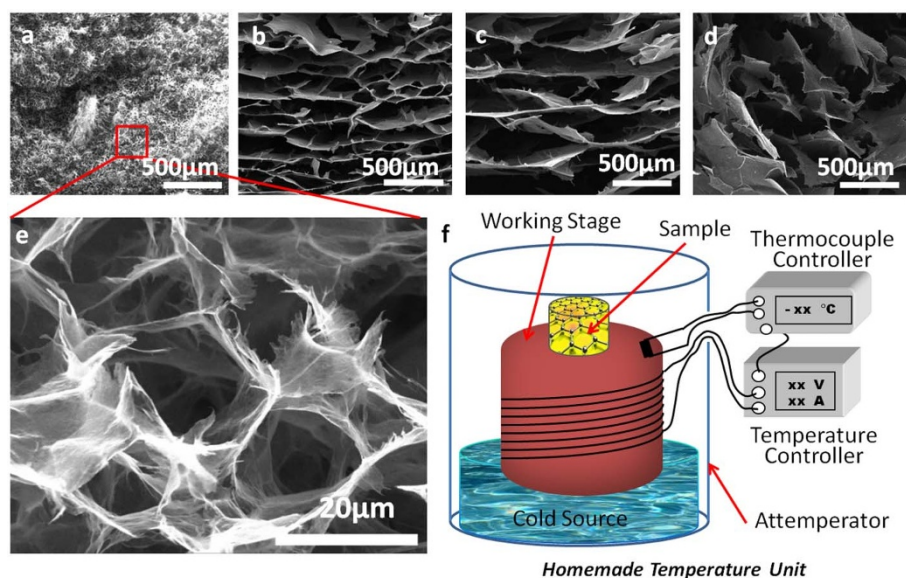


Figure 1 | Microstructures of sponge graphenes frozen at different temperatures. (a–d) SEM images of the porous structure of four graphene sponges fabricated at different freezing temperatures of -170 , -40 , -20 , and -10°C . Scale bar: $500\ \mu\text{m}$. (e) High-magnification SEM image of the pore walls composed of graphene nanosheets corresponding to panel a. The mean thickness of the pore walls is $10\ \text{nm}$ (detailed images for the other temperatures are available in Supplementary Information). (f) Working schematic of the homemade freezing temperature unit.

most important role in regulating the microporosity. Moreover, the water absorption/resistance properties of the porous structure is closely depended on the pore size.

Results

Freezing temperature and microstructure of graphene sponges. A series of graphene sponges was fabricated using the protocol described in the Methods Section. Briefly, GO dispersion obtained from the oxidation of graphite was hydrothermally reduced to hydrogel and then treated with freeze drying under different temperatures. The entire working flow in detail is demonstrated as Supplementary Fig. S1. The final products are $14\ \text{mm} \pm 1\ \text{mm}$ in diameter and $15\ \text{mm} \pm 1.5\ \text{mm}$ in height. The density of the sponges was measured to be approximately $10\ \text{mg cm}^{-3}$ (including the air inside the sponge), despite the alterable microstructures that will be discussed afterward.

Figure 1 describes the horizontally cut cross-sectional morphology of sponge blocks subjected to different freezing temperatures. Figures 1a to 1d correspond to freezing temperatures of -170 ,

-40 , -20 , and -10°C , respectively. The micropores become denser and the pore size decreases as the temperature of the cold source decreases. Figure 1e shows the magnified pore walls of the sponge in Fig. 1a. Magnified details of pore walls under other freezing temperatures can be found in Supplementary Fig. S2. Figure 1f demonstrates the schematic of the homemade temperature unit for freezing temperature control. Briefly, a cylindrical copper bar was twined with resistance coils and immersed in the cold source (liquid nitrogen) inside an attemperator. The thermocouple measures the temperature on the working stage and outputs a feedback signal to the temperature controller to decide the heating power on the coil. A statistics of the mean pore size and wall thickness at the different freezing temperatures is demonstrated in Fig. 2a and 2b. As can be seen, the pore size increases by 70 times, e.g., from 10 – $15\ \mu\text{m}$ at -170°C to 700 – $800\ \mu\text{m}$ at -10°C . Thickness of the pore wall in Fig. 1e is only $20\ \text{nm}$. Wall thickness increases dramatically when the freezing temperature is elevated (see Supplementary Fig. S2), e.g., wall thickness increases up to $80\ \mu\text{m}$ at -10°C freezing temperature, which is approximately 8000 times thicker than that at -170°C . A large-range regulation of

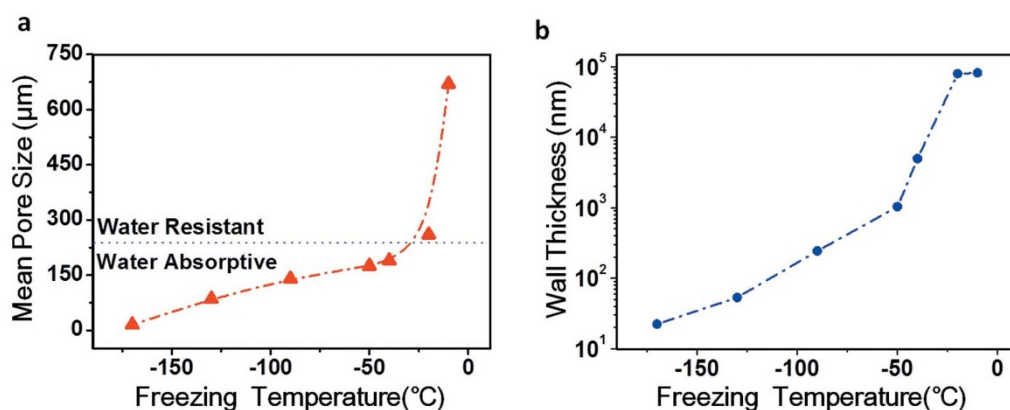


Figure 2 | Statistics of the average a, pore size and b, wall thickness as a function of freezing temperature. Mean pore size varies from $10\ \mu\text{m}$ to $700\ \mu\text{m}$ with corresponding freezing temperatures of -170°C and -10°C , while the wall thickness increases from $20\ \text{nm}$ to $80\ \mu\text{m}$, respectively. The mean micropore size on the surface determines whether the surface absorbs water according to n individual batches of sponges ($n > 12$). Pores with sizes ranging from $250\ \mu\text{m}$ to $700\ \mu\text{m}$ show water resistance, whereas pores smaller than $250\ \mu\text{m}$ allow water absorption.



the porosity has been thus realized simply by controlling the freezing temperature. It should be pointed out that, the cut plane of graphene sponges may lead to different observations because high freezing temperatures generate anisotropic structures, i.e., the ice crystal grows along the direction of the temperature gradient. More isotropic structures can be formed in liquid nitrogen.

In addition, the porous morphology changes from cellular to lamellar with increasing freezing temperature (Supplementary Fig. S3). This result may be attributed to the change in the crystal shape of ice. Several parameters may affect the microstructures in graphene sponges, such as solvent, pH, solution concentration, and freezing condition. A previous study has discussed the effect of pH in detail¹³. Freezing rate, which decides the rate of ice crystallization and growth, is recognized as the most critical factor affecting the morphology of the microcells in the sponge during freeze casting. By controlling the temperature of the cold source, structural evolution is explored. Therefore, determining the tailoring effect of freezing temperature on sponge porosity is necessary.

Ice solidification comprises two individual but consecutive phases: nucleation and growth of ice crystals. In addition, a competitive balance exists between the two phases. A large temperature gradient may increase nucleation rate and suppress growth¹⁹. Therefore, assuming that the room temperature is invariant, a large temperature gradient along the solidification direction from the cold source to the samples is generated by decreasing the temperature of the cold source. As a result, a high rate of ice solidification is obtained. As shown in Fig. 3, a low ice solidification rate (e.g., small temperature gradient or high freezing temperature) yields large ice crystals, with more graphene dispersions accumulating between ice crystals. Conversely, more graphene dispersions suspended in water are repelled during crystal formation. Thus, porous structures with large pore sizes and thick graphene walls are obtained. By contrast, a high ice solidification rate (e.g., high temperature gradient or low freezing temperature) yields small spacing and thin walls. However, an excessively slow ice solidification rate generates sponges with extremely large pore sizes, which may lead to sponge block collapse. For example, graphene dispersion slowly frozen in a commercial refrigerator from room temperature to -20°C appears like scattered flakes and cannot form an intact shape.

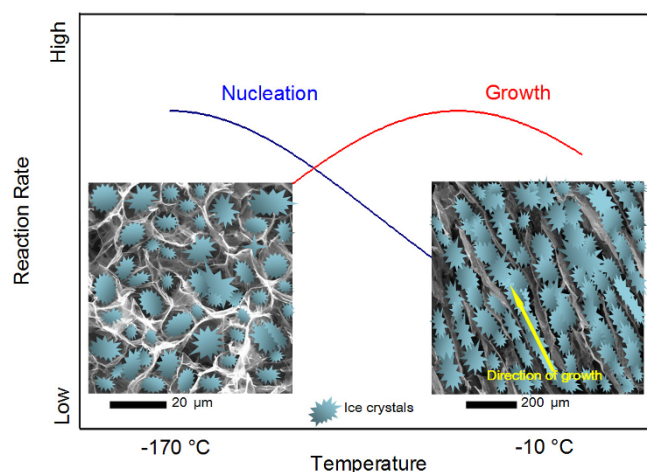


Figure 3 | Qualitative schematic of the relationship between nucleation and crystal growth as a function of freezing temperature during ice solidification. At low temperatures, nucleation dominates the process; at high temperatures, crystal growth is favored. The size of ice crystals is not drawn proportionally to that of a graphene sponge. Ice crystals are demonstrated artificially on the background, the factual SEM images of microstructures.

Water absorption on the cross-section of the graphene sponges.

Graphene-based porous materials often contacts with liquid environment in many applications, for instance, electrodes and sorbent materials. Therefore, whether the surface of a graphene sponge absorbs water should depend on specific usage. For example, when used as electrodes in a supercapacitor, graphene sponges should have a sufficient water absorption to increase the contact probability of the ions and dyes in the electrolyte. However, as sorbent which eliminates liquid contaminations, the graphene sponge should be water resistant. In this case, water absorption hinders the absorptive capacity of the sponge to organic chemicals and causes difficulty in the consequent recycling. The effect of graphene sponge sorbent could be found in our previous studies¹³. In other literatures regarding oil removal, many other porous materials were often pre-processed first with surface modification in order to be water resistant, which dramatically decreases the absorbance capacity of these materials to oils²⁰. To clarify the relationship between the microstructures of sponges and their performance in water absorption, sponges fabricated at different freezing temperatures (-10 , -20 , -30 , -40 , -50 , and -170°C) were selected for comparative study. The porous microstructures were then inspected by scanning electron microscopy (SEM). Water absorption on freshly prepared cross-sections of the sponges was tested for different positions. Figure 4 shows the performance of the sponges.

Elemental analysis of the cross-sectional surface of these sponges by X-ray photoelectron spectroscopy (XPS) shows no significant difference (see Supplementary Fig. S4). The atomic concentrations calculated from the spectra are $83.7\% \pm 4.2\%$, $6.3\% \pm 1.72\%$, $9.8\% \pm 2.0\%$, and $0.2\% \pm 1.5\%$ for C(1s), O(1s), N(1s), and S(2p), respectively. Therefore, the determining factor of water absorption of a graphene sponge is their microstructures, specifically, the mean pore size. Freezing at temperatures higher than -20°C produces pores larger than $300\ \mu\text{m}$, causing the sponge water resistant. By contrast, freezing at temperatures lower than -50°C produces pores smaller than $150\ \mu\text{m}$, causing the sponge to be water absorbent. Freezing at transitive temperatures (e.g., -40°C to -20°C) brings the possibility that some positions on the surface (around the center) are water absorbent whereas other positions (at the edge) are water resistant. In this case, an uneven temperature gradient when preparing the

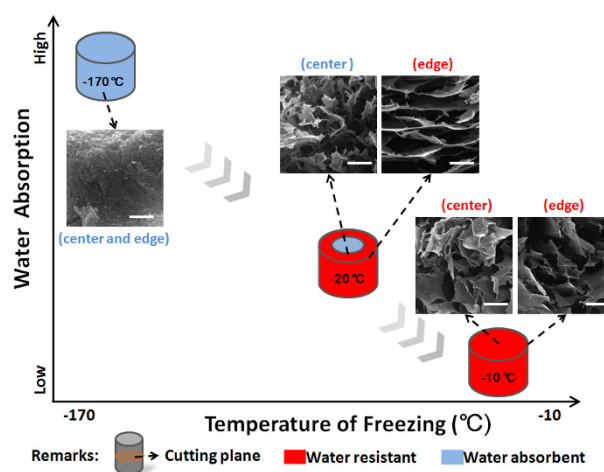


Figure 4 | Performance of water absorption/resistance on the cross-section of a sponge. The as-prepared surfaces become water absorbent at low freezing temperatures during fabrication. A cross-section may also possess different water absorption properties in the center and near the edge at transitive freezing temperatures, e.g., -20°C . The SEM images indicate the corresponding microstructures of the surface. Scale bars: $500\ \mu\text{m}$.



sponges is regarded as the cause of inhomogeneous freezing of the sponge body. Significant differences in surface morphology could be observed through SEM. Cabbage-like microstructure is typically observed in the water-resistant region, whereas smaller pore sizes, better uniformity and finer textures are generally for the water-absorbent region.

Mechanical property (compressive deformation). Aside from oil absorption, the microstructures strongly affect the mechanical properties of graphene sponges. As a novel material, the mechanical properties of three-dimensional porous carbon materials are usually characterized with compressive stress-strain curves as well as Young's Modulus^{3,19,21}. Figure 5a records the generated stress as a function of compressive strain for the as-prepared sponges. The stresses deviate from Hooke's law (dash lines in Fig. 5a) when raising the strain, indicating a greater plastic proportion during larger structural deformation. Specifically, for the -170°C sponges, plastic deformation becomes dominant when the strain is larger than 5%. For a comparative study, elastic deformation in this work is defined in the range of the strain smaller than 5% (grey region in Fig. 5a) for all sponges. The Young's Modulus are then calculated as 204.4 and 13.7 KPa for the -170°C and -20°C sponges, respectively (Fig. 5a, inset). The results are comparable to a previous work²¹, or are slightly higher than previous literatures reporting porous carbon structures³. Moreover, all the sponges show stress drops at different critical stresses, indicating the partial release of stress through plastic deformation of the inner structures. Therefore, sponges with elastic modulus varied by 15 times can be obtained simply by varying freezing temperatures. Figure 5b demonstrates the sponge recovery after 10 cycles of compression under 1 N weight (~ 7 KPa pressure). For all the sponges, a permanent plastic deformation is observed at the first cycle. The level of plastic deformation in the first cycle reflects the damage of the inner structure, and the volume recoveries of the -170°C and -20°C sponges after the first cycle are 95% and 78%, respectively (the volume before compression has been normalized to 100%). Deformation stabilizes, indicating that elastic deformation dominates the subsequent cycles. Moreover, after the ostensible recovery of the sponges, the inner microstructure of the -20°C sponge is partially broken into flakes, whereas the -170°C sponge retains its fine, cellular structure as shown in Fig. 1a. This finding may be attributed to the fact that isotropic, thinner cell walls ensure abundant cross-linkage among single graphene nanosheets to disperse the unidirectional pressure into all directions, making it

stiffer and more difficult to be destroyed. The corresponding video clips showing the compressive deformation of the -20°C and -170°C graphene sponges are provided in Supplementary Movies S1 and S2. The mechanical properties of the isotropic structure obtained with liquid nitrogen freezing may provide a potential to acquire highly elastic graphene aerogels.

Discussion

In this study, we have found that ice solidification rate affects the morphology of micropores. In ice solidification, a competitive mechanism exists between ice nucleation rate and growth rate, which correspond to the shape of the sponge pores. The initial nucleation of ice crystals is a stochastic process. However, the ice crystal always grows along the direction of the temperature gradient after nucleation. During freezing at relatively high temperatures, crystal growth is more preferable than nucleation, resulting in large anisotropic, lamellar ice crystals parallel to the solidification direction. After being dried, the sponge block shows a cabbage-like cross-section with lamellar cell walls which are parallel to the cold source and are concentric around the block center (Fig. 1c and Supplementary Fig. S3). By contrast, during freezing at low temperatures (e.g., liquid nitrogen), the dominant process is nucleation. When the bottom of graphene hydrogel comes in contact with liquid nitrogen without any temperature compensation, the temperature drops so sharply that nucleation occurs instantaneously everywhere and crystal nuclei occupy the entire gel. Therefore, neither time nor space is available for the lamellar growth of ice crystals. High porosity with homogeneous, small cells reflect high nucleation rate while suppressing the effect of anisotropic growth of ice crystals (Fig. 1c and Supplementary Fig. S3). Although it has been reported that the porosity could be controlled by freeze casting in the fabrication of porous materials, e.g. ceramics, it is for the very first time that such a large-range of porosity regulation, e.g. by several thousand times, has been ever reported. The mechanism inside the large-range regulation is yet to be discovered.

During freezing, the graphene nanosheet is preferably pushed away from the ice front to participate in the self-assembly of pore walls instead of remaining in its initial position in the ice crystal, forming thicker pore walls with an elevated temperature. However, an explanation for this phenomenon remains absent. If graphene prefers stay in its initial position during ice growth, slight morphological differences under various freezing temperatures can be observed. In fact this phenomenon can be explained by both the

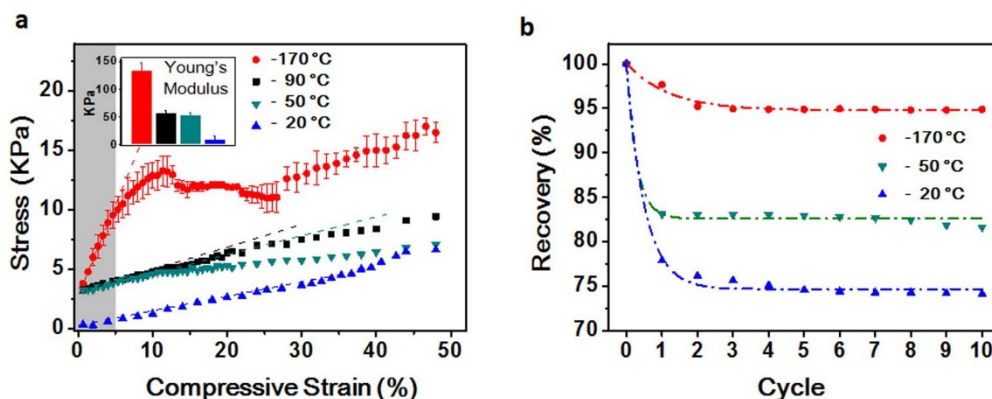


Figure 5 | Mechanical property (compression) of the as-prepared sponges. (a) Stress as a function of compressive deformation. The corresponding dash lines shows the linear direction of the curve which obeys Hooke's law. The region with grey background illustrated the elastic deformation of the sponges ($<5\%$). Inset: The -170°C sponge shows a compressive modulus of 204.4 KPa, which is approximately 15 times higher than that of the -20°C sponge (13.7 KPa). $n > 3$. (b) Recovery of the sponges after repetitive compression-release cycles. The deformation stabilized after the first cycle, in which permanent plastic deformations of 95% and 78% are observed for the -170°C and -20°C sponges, respectively. The volume of the sponge before compression was normalized to 100% (cycle 0). The dynamic process of mechanical compression release could also be found in Supplementary Information.



interfacial energy and the hydrophobic nature of graphene. On the one hand, an ice front (water–ice interface) always exists during growth of ice crystals. Therefore, the interface may be considered to be composed of a layer of ice lattice and another layer of water molecules. Based on the lowest energy principle, the interface prefers to absorb external water molecules to form ice crystals rather than graphene nanosheets that may lead into irreversible lattice mismatch on the water–ice interface and thus raise the interfacial energy.

On the other hand, knowing that graphene is a hydrophobic material, the graphene fraction in water dispersion without any stabilizer aggregates driven by hydrophobic interactions. Therefore, during crystal growth, graphene nanosheets are spontaneously repelled by the ice front to form thicker, more solid pore walls rather than dispersing in ice crystals.

The phenomenon of water absorption/resistance on the surface can be explained by the theory of surface wettability, i.e., a non-wettable surface cannot absorb water from the solid–liquid interface. Surface wettability is generally considered to be affected by both the intrinsic nature of the material and the microstructures. We have demonstrated that the sponge surface containing pores smaller than 250 μm tends to be water absorbent. According to the classical Cassie–Baxter's model, the wettability of a surface is affected by the nature of solid and air phases and their corresponding proportions on the surface:

$$\cos \theta_{cb} = \Phi_S \cos \theta_S + \Phi_A \cos \theta_A \quad (1)$$

where θ_{cb} is the contact angle of the apparent surface. θ_S and θ_A are the contact angles of the solid phase and air phase which composes the entire surface, respectively. Φ_S and Φ_A are the percentages of surface area of the solid and air phases on the entire surface, respectively. In the case of graphene sponge, we have $\Phi_S = 1 - \Phi_A$, and the contact angle of water in the air is always assumed as 180° . Therefore, equation (1) can be simplified as follows:

$$\cos \theta_{cb} = \Phi_S (\cos \theta_S + 1) - 1 \quad (2)$$

We attempted to explain this phenomenon semi-quantitatively because the precise contact angle of water on graphene is highly affected by complex parameters (e.g., layer thickness, substrate type, etc.) and is still disputable. Fortunately, the graphene layer itself is a well-known as a highly hydrophobic material. Thus, $\cos \theta_S$ is a negative constant between -1 and 0 . A large Φ_S value indicates that $\cos \theta_{cb}$ converges toward 0 . Therefore, when the cross-sectional interface of a graphene sponge becomes denser, the surface becomes more hydrophilic than when it has larger pores. This interpretation indicates that moderately refining the porous microstructure of the cross-section of a graphene sponge could improve its water wettability. These theories are consistent with the observations in the experiments. As shown in Figs. 1 and 2, the microstructure of the cross-section becomes more compact when decreasing the freezing temperature. As shown in Fig. 2a, a range of freezing temperatures produces proper pore sizes below 250 μm , yielding graphene sponges with water-absorbent surfaces. Therefore, we demonstrate that the microstructure and water absorption property of a graphene sponge could be freely controlled by regulating the freezing temperature. To obtain water-friendly sponges, the freezing temperature for the graphene hydrogel should be controlled below -50°C . Conversely, the freezing temperature could be safely set above -20°C in order to fabricate graphene sponges that are suitable to be applied as oil sorbent.

In conclusion, freeze casting, especially freezing temperature, is a critical factor that affects the porosity of graphene-based 3-D structures. This study focused on tailoring the microstructure and corresponding properties of graphene sponges by varying the freezing temperature. A homemade freezing temperature control unit was applied to obtain precise freezing temperature of the ice solidification inside the graphene sponge. By decreasing the freezing temperature,

both pore size and pore wall thickness decrease within a wide range by 80 and 4000 times, respectively. The pore morphology changes dramatically, from anisotropic, lamellar to uniform, cellular structures. The mechanism is attributed to the combination of the interfacial energy and hydrophobic nature of the graphene material. Moreover, the change in absorptive performance of water can be explained by the gradually microstructural evolution. The mechanical property, especially the elastic deformation of graphene sponges, was also studied. The Young's Modulus of the sponge can also be greatly varied by 15 times (from 13.7 to 204.4 kPa). Various properties of graphene sponges can be regulated by controlling the freezing temperature, e.g., water-absorbent sponges may help for electrodes in ionic liquids, whereas water-resistant sponges can be applied as oil remover. This study is believed as a basis for the large range controllable, template-free preparation of porous graphene. Our results may also be suitable for other applications, such as solvent removal during graphene transfer on solid-state substrates²².

Methods

Synthesis of graphite oxide and GO dispersion. A modified Hummers method was employed to fabricate graphite oxide; the detailed process can be found in our previous reports^{23,24}. Dried solid-state, dark brown graphite oxide powder was redissolved in deionized water and ultrasonicated for 1 h. The dispersion was centrifuged at 10,000 g, and GO dispersion was obtained by discarding the precipitate.

Fabrication of a hydrothermal-reduced GO (HRGO) gel block. An HRGO gel block was fabricated according to the hydrothermal reduction. A previous study reported that pH 10 is the optimum condition for gel aggregation and excellent quality. Therefore, during the reduction, the pH of the remaining dispersion was tuned to 10^{24} . GO (60 mg) was dissolved in 20 mL distilled water and then ultrasonicated until a homogeneous dark brown colloidal dispersion was obtained. Subsequently, 0.5 mL ammonia (30 v/v%) was added and stirred evenly. The GO dispersion (3 mg mL⁻¹) was transferred into a sealed reactor with a cylindrical Teflon container. The reactor was heated to 180°C for 20 h and then cooled down to room temperature mildly. Finally, a wet, black cylindrical HRGO gel block was obtained.

Freezing and vacuum drying of the HRGO block. The HRGO block was placed on a metal tray, which was then transferred to a cold source with constant temperature. The rate of crystal growth was controlled by regulating the temperature of the cold source. Freezing lasted for several minutes until the gel block was fully solidified. Temperatures above -50°C can be achieved directly by applying cold traps to the freeze dryer (Model: LGJ-10D, Beijing Sihuan Scientific Ltd., China). Low temperatures were achieved using the homemade temperature control unit, as described below. One end of a copper bar was immersed in liquid nitrogen, whereas the other end was used as the cold source. A resistance wire and a thermocouple were wound on the bar to control the temperature of the cold source (Fig. 1f). The lowest temperature -170°C was obtained by liquid nitride without heating. After the gel was completely frozen, the samples were placed in a freeze dryer for 48 h, generating black graphene sponges. The final working temperature in the freeze dryer was set to 45°C in order to completely remove the solvent, and the final air pressure was kept lower than 10 Pa. The volume of monoliths at the laboratory level is $\sim 6 \text{ cm}^3$ with a corresponding cost of $\sim \$0.3$ per gram. The volume will be easily scaled up and the cost further decreased once the protocol can be transferred into massive production in industry.

Characterization of the graphene sponges. The surface morphology of the sponges was characterized using a scanning electron microscope (Quanta 200, FEI, USA) operated at a high voltage of 20 kV. Images of the inner structure were also characterized by SEM by horizontally cutting the sponge blocks. The chemical composition of the cross-section of the sponges was determined via XPS (PHI 5000 VersaProbe, UIVAC-PHI, Japan).

Water absorption and mechanical performance. At room temperature, a drop of water ($\sim 20 \mu\text{L}$) was dripped onto a freshly, horizontally cut cross-section of a graphene sponge. Whether the plane absorbs water was determined by 3 minutes of observation. Different regions on the same cutting plane, e.g. the center and the edge, were tested to show different water resistance levels. The mechanical properties of the sponges were tested using a mechanical test stand (SHAHE SML-J, China) and a dynamometer (SHAHE SH-50, China). The sponges were compressed to a specific strain, e.g., 10%, and the generated stress was measured. The curves in Fig. 5 were then calculated based on these data, and the Young's Modulus of the sponges was calculated with the known height and diameter of the sponges.

- Geim, A. K. Graphene: status and prospects. *Science* **324**, 1530–1534 (2009).
- Novoselov, K. S. *et al.* A roadmap for graphene. *Nature* **490**, 192–200 (2012).



3. Mecklenburg, M. *et al.* Aerographite: ultra lightweight, flexible nanowall, carbon microtube material with outstanding mechanical performance. *Adv. Mater.* **24**, 3486–3490 (2012).
4. Zhu, Y. W. *et al.* Graphene and graphene oxide: synthesis, properties, and applications. *Adv. Mater.* **22**, 3906–3924 (2010).
5. Murali, S. *et al.* Preparation of activated graphene and effect of activation parameters on electrochemical capacitance. *Carbon* **50**, 3482–3485 (2012).
6. Chen, W. F. & Yan, L. F. In situ self-assembly of mild chemical reduction graphene for three-dimensional architectures. *Nanoscale* **3**, 3132–3137 (2011).
7. Worsley, M. A. *et al.* Synthesis of graphene aerogel with high electrical conductivity. *J. Am. Chem. Soc.* **132**, 14067–14069 (2010).
8. Zhang, X. *et al.* Mechanically strong and highly conductive graphene aerogel and its use as electrodes for electrochemical power sources. *J. Mater. Chem.* **21**, 6494–6497 (2011).
9. Chen, J., Sheng, K. X., Luo, P. H., Li, C. & Shi, G. Q. Graphene hydrogels deposited in nickel foams for high-rate electrochemical capacitors. *Adv. Mater.* **24**, 4569–4573 (2012).
10. Zhu, Z. *et al.* A critical review of glucose biosensors based on carbon nanomaterials: carbon nanotubes and graphene. *Sensors* **12**, 5996–6022 (2012).
11. Singh, G. *et al.* ZnO decorated luminescent graphene as a potential gas sensor at room temperature. *Carbon* **50**, 385–394 (2012).
12. Zhao, J., Ren, W. & Cheng, H.-M. Graphene sponge for efficient and repeatable adsorption and desorption of water contaminations. *J. Mater. Chem.* **22**, 20197–20202 (2012).
13. Bi, H. *et al.* Spongy graphene as a highly efficient and recyclable sorbent for oils and organic solvents. *Adv. Funct. Mater.* **22**, 4421–4425 (2012).
14. Deville, S. Freezing as a path to build complex composites. *Science* **311**, 515–518 (2006).
15. Sofie, S. W. & Dogan, F. Freeze casting of aqueous alumina slurries with glycerol. *J. Am. Ceram. Soc.* **84**, 1459–1464 (2001).
16. Mukai, S. R., Nishihara, H. & Tamon, H. Formation of monolithic silica gel microhoneycombs (SMHs) using pseudosteady state growth of microstructural ice crystals. *Chem. Commun.* **7**, 874–875 (2004).
17. Nishihara, H., Mukai, S. R., Yamashita, D. & Tamon, H. Ordered Macroporous Silica by Ice Templating. *Chem. Mater.* **17**, 683–689 (2005).
18. Zou, J. *et al.* Ultralight Multiwalled Carbon Nanotube Aerogel. *Acc Nano* **4**, 7293–7302 (2010).
19. Li, W. L., Lu, K. & Walz, J. Y. Freeze casting of porous materials: review of critical factors in microstructure evolution. *Inter. Mater. Rev.* **57**, 37–60 (2012).
20. Li, S. D. *et al.* Vaseline-loaded expanded graphite as a new adsorbent for toluene. *Chem. Eng. J.* **162**, 546–551 (2010).
21. Sun, H., Xu, Z. & Gao, C. Multifunctional, ultra-flyweight, synergistically assembled carbon aerogels. *Adv. Mater.* **25**, 2554–2560 (2013).
22. Meyer, J. C. *et al.* The structure of suspended graphene sheets. *Nature* **446**, 60–63 (2007).
23. Hummers, W. S. & Offeman, R. E. Preparation of graphitic oxide. *J. Am. Chem. Soc.* **80**, 1339–1339 (1958).
24. Bi, H. *et al.* Low temperature casting of graphene with high compressive strength. *Adv. Mater.* **24**, 5124–5129 (2012).

Acknowledgments

This work was supported by the National Basic Research Program of China (Grant Nos. 2011CB707601 and 2009CB623702), the National Natural Science Foundation of China (Nos. 61274114, 11204034 and 51071044), the Natural Science Foundation of Jiangsu Province (Nos. BK2012024 and BK2012123), Scientific Research Foundation of Graduate School of Southeast University (No. YBJJ1208) and funds from Ministry of Education.

Author contributions

L.T.S. proposed and supervised the entire project. X.X., Y.L.Z. and K.B.Y. performed the experiments. H.C.B. and S.W. assisted with the preparing materials and improving the method for the study. L.T.S., X.X. and Y.L.Z. analysed data and wrote the manuscript, and all the authors participated in discussions of the research.

Additional information

Supplementary information accompanies this paper at <http://www.nature.com/scientificreports>

Competing financial interests: The authors declare no competing financial interests.

How to cite this article: Xie, X. *et al.* Large-range Control of the Microstructures and Properties of Three-dimensional Porous Graphene. *Sci. Rep.* **3**, 2117; DOI:10.1038/srep02117 (2013).



This work is licensed under a Creative Commons Attribution-NonCommercial-ShareAlike 3.0 Unported license. To view a copy of this license, visit <http://creativecommons.org/licenses/by-nc-sa/3.0>